Progress In Electromagnetics Research C, Vol. 100, 205–218, 2020

HEMP Excited Shield Residual Electric Field Modeling Method Based on NARX Neural Network

Zhizhen Zhu*, Jing Yang, Yuewu Shi, Xin Nie, Linshen Xie, Wei Wang

Abstract—To predict the residual electric field inside an electromagnetic (EM) shield under illumination of different HEMP waveforms, a method based on NARX neural network is proposed in this paper. The model can be established from input-output data of EM shield without knowing enclosure and internal structural details. To evaluate the precision of the prediction method, two error criteria based on energy and field amplitude are provided in this paper. As a numerical example, the double exponential pulse with 10% to 90% rise time of 2.5 ns, the pulse width at half maximum of 23 ns, and the corresponding residual electric field are taken as the training data. The EM simulation is used to establish the model of residual electric field inside the shield. The NARX neural network is then built and trained. Other double exponential pulses, with different rise times and pulse widths, and their residual field are taken as the checking data. The results show that the error of the prediction method is sufficiently small for actual use.

1. INTRODUCTION

High-altitude Electromagnetic Pulse (HEMP) can cause interference and even serious damage to electronic systems [1]. With the development of electronic technology, integrated circuit size shrinks from micrometers into nanometers. The integrated circuit with lower power consumption becomes more complicated in scale. HEMP poses a greater threat to electronic systems, such as radar [2] and electronic systems [3].

Shielding is one of the most widely used and effective HEMP protection methods [4]. The internal residual electric field of EM shield is commonly used to characterize the protection effect on HEMP. Obviously, it is better to have a smaller residual electric field. Material, structure, and characteristics of EM shield will affect the residual electric field [5]. At present, the residual electric field inside EM shield is obtained mainly by HEMP field tests or numerical simulations. However, for traditional numerical methods, such as FDTD [6, 7], MOMs [8], FEM [9], and analytical geometry methods [10], the precise results are based on the assumption that the aperture can be measured and modeled precisely which in fact is difficult due to the complexity of welds and other actual non-ideal factors. For HEMP field tests, only limited results can be provided. The tests of the shield rely on large-scale HEMP simulators [11] which are scarce resources with high costs and long test cycles. If the prediction of the residual electric field under other illumination environment is required, the shielding effectiveness curve of the shield is calculated in frequency domain by the measurement result, and then the minimum phase method is used to predict. The method produces deviation due to the loss of phase information during the data processing.

Artificial neural network has a strong ability of solving complex and nonlinear problems. [12] and [13] have already applied artificial neural network (ANN) to handle the shielding effectiveness (SE)

Received 13 January 2020, Accepted 9 March 2020, Scheduled 26 March 2020
* Corresponding author: Zhizhen Zhu (zhuzhizhen@nint.ac.cn).
The authors are with the State Key Laboratory of Intense Pulsed Radiation Simulation and Effect (Northwest Institute of Nuclear Technology), Xi'an 710024, China.

of rectangular enclosure with apertures. In [12], the authors use ANN to predict the electric field strength inside a metallic shield. The electric field strength of different rotation angles and radiation power levels can be predicted with the method. In [13], two kinds of neural networks (MLP and RBF) are proposed to simultaneously estimate the SE. The models have good generalization capability and show a good estimation accuracy. However, in these methods, ANN is only applicable to the estimation of one or two parameters of the shield. The waveform inside the enclosure cannot be estimated. And the information provided is very limited.

In this paper, EM shields are modeled by NARX neural network. The experimental measurement results are used to train the model. It can be used to predict the residual electric field inside the shield under the illumination of other HEMP or EMP waveforms. To evaluate the precision of the prediction method, two error criteria are proposed in this paper. The results show that the prediction results of the NARX neural network are basically consistent with the electromagnetic results of numerical simulations or HEMP field tests, and the error is sufficiently small for application. The NARX neural network based method combines the advantages of HEMP field test and numerical simulation. It can provide prediction without the requirement of accurate modeling due to the use of real experimental measurement results.

2. HEMP ENVIRONMENT

HEMP is in the form of a double exponential wave, as shown in Eq. (1) [14].

$$E(t) = K\left(\mathrm{e}^{-\alpha t} - \mathrm{e}^{-\beta t}\right) \quad (t \geq 0) \tag{1}$$

where parameters K, α, β are constant, regardless of time t. There is $0 < \alpha < \beta$ to ensure that $E(t)$ is positive.

The normalized waveform of HEMP is shown in Fig. 1. The 10–90% rise time and pulse width at half maximum of the waveform are represented by t_r and t_w, respectively.

The different HEMP waveform parameters involved in this paper are: (1) The waveform parameters of the IEC 61000-2-9 [14]: $t_r = 2.5\,\mathrm{ns}$, $t_w = 23\,\mathrm{ns}$, the corresponding parameters are: $\alpha = 4.0 \times 10^7$, $\beta = 6.0 \times 10^8$, $K = 6.5 \times 10^4$; (2) Bell HEMP waveform parameters [15]: $t_r = 4.1\,\mathrm{ns}$, $t_w = 184\,\mathrm{ns}$, the corresponding parameters are: $\alpha = 4.0 \times 10^6$, $\beta = 4.76 \times 10^8$, $K = 5.25 \times 10^4$; (3) The waveform parameters of the international academic publications in 1976 [16]: $t_r = 7.8\,\mathrm{ns}$, $t_w = 483\,\mathrm{ns}$, the corresponding parameters are: $\alpha = 1.5 \times 10^6$, $\beta = 2.6 \times 10^8$, $K = 5.2 \times 10^4$. Various HEMP waveforms are shown in Fig. 2.

HEMP environment is generated by an HEMP simulator. In an HEMP field test, the system under test (SUT) is placed in the working volume of the HEMP simulator. During the test, EM environment,

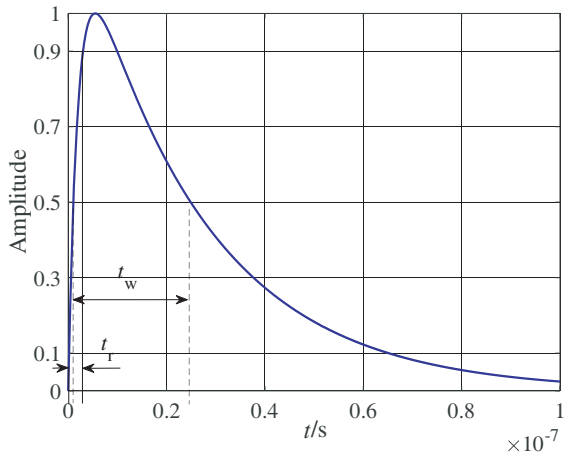

Figure 1. Normalized waveform of HEMP.

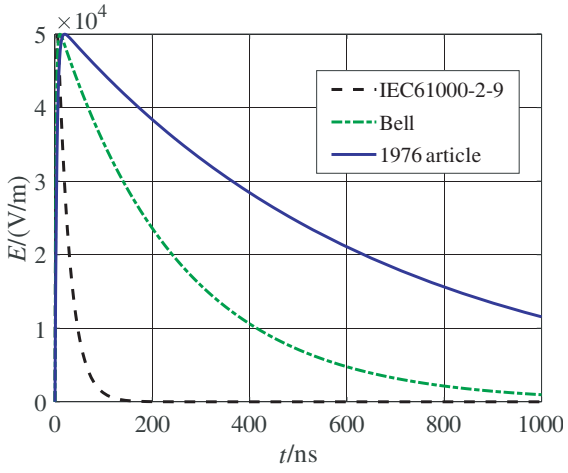

Figure 2. HEMP waveforms specified by different standards.

coupling current and voltage on cables, and coupling field inside shields are measured. Field, current and voltage sensors are placed at certain predesigned locations. Before and after each illumination of the simulated HEMP, the state and operating data of the SUT are checked and documented. All the test data will be used for evaluation of the SUT.

3. PREDICTION MODEL BASED ON NARX NEURAL NETWORK

The method in this paper is based on an Artificial Neural Network (ANN), which is a combination of testing and theoretical modeling. The method uses experimental data for modeling and predicting, without the requirement to accurately model the structure of EM shield. The whole modeling process regards EM coupling in actual problem as "black box". Under a specified neural network structure, the parameters of the network are trained from the input and output of the actual system. Compared to the traditional EM method, it does not require the detail information about the EM shield.

3.1. NARX Neural Network

Dynamic neural network is a commonly used time series prediction algorithm. The NARX neural network is a nonlinear autoregressive with exogenous inputs model. For the approximation ability of dynamic systems, the NARX neural network is much stronger than general static neural networks. Its dynamic behavior is shown in Eq. (2) [17].

$$y'(t+1) = f(x(t), \cdots, x(t-m), y(t), \cdots, y(t-n)) \tag{2}$$

where $f(\cdot)$ is a nonlinear function of all independent variables, and $x(t)$ and $y'(t)$ are the input and output signals of the neural network. The structure of NARX neural network is shown in Fig. 3, where m and n are the time delays of $x(t)$ and $y(t)$, respectively.

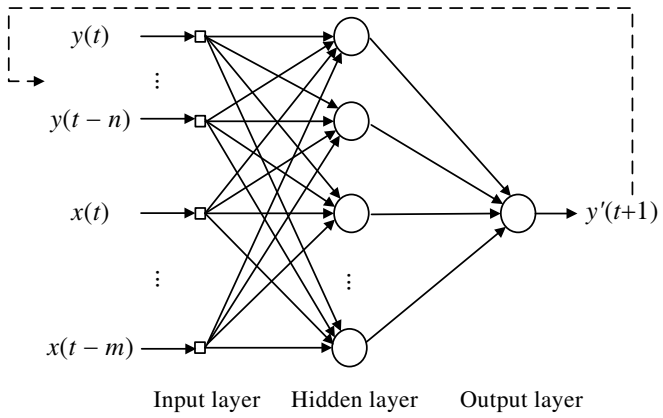

Figure 3. Schematic diagram of NARX neural network.

In this paper, the nonlinear activation function of the hidden layer uses the logsig function $y = \log\mathrm{sig}(x) = 1/(1+\mathrm{e}^{-x})$. The nonlinear activation function of the output layer is chosen as purelin, which is the most common linear transfer function. The structure of NARX neural network uses a series-parallel architecture. The learning algorithm adopts Bayesian Regularization (BR) algorithm [18]. It possesses good ability of generalization capacity. In the training process, the algorithm regards the network weight and node threshold as random variables. The parameters are adjusted according to their probability density function. On the one hand, the algorithm makes the network error as small as possible. On the other hand, it reduces the scale of the network. If the sample size is set as constant, the network scale is much smaller than the sample size, which effectively reduces the possibility of over-fitting. The generalization performance of neural networks is also enhanced.

Since NARX neural network [19] and BR algorithm [20–22] are mature methods, the detailed descriptions are not elaborated in this paper.

3.2. NARX Neural Network Modeling Process

Step 1: Obtain training data.

The waveform of the simulated HEMP field and the corresponding internal residual electric field signal are respectively used as input and output training data of the network. According to the basic theory of signal, it is required that the training signals satisfy Nyquist sampling theorem; otherwise, the waveforms cannot be correctly represented due to aliasing. In one test, the sampling intervals of the input and output training data are commonly same with each other. At the same time, the spectrum of the training illumination waveform should cover the spectrum of the illumination waveform in prediction. Otherwise, the neural network will not be able to correctly complete the prediction due to lack of information of the corresponding spectrum. In this paper, this basic requirements of spectrum coverage can be met between the different HEMP waveforms, as shown in Fig. 4.

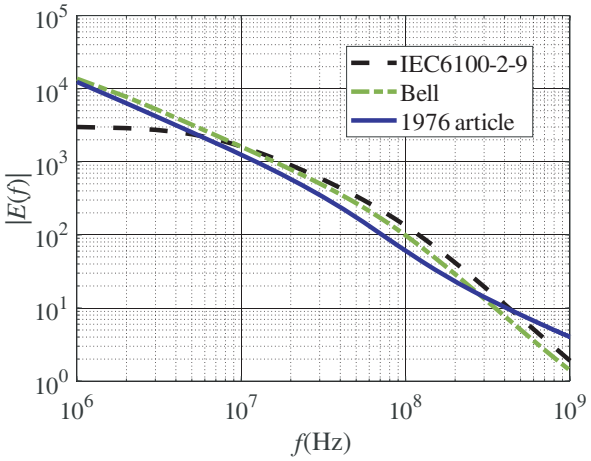

Figure 4. Spectrum coverage between the different HEMP waveforms.

Step 2: Establish a NARX neural network.

In order to establish the NARX neural network, there are several works to do: select the time delay, determine the number of neurons in each layer and the connection of neurons. The longer the time delay is, the stronger the network's ability to model complex systems will be, and the more accurate the prediction results will be. However, the system complexity and training time are increased at the same time. With the same number of iterations, performance can deteriorate. On the contrary, the shorter the time delay is, the simpler the network will be, and the shorter the training time will be. However, the modeling ability is correspondingly poorer because of the difficulty in convergence and under-learning. Therefore, it is necessary to repeatedly analyze the process and results of simulations, and gradually select the appropriate time delay and the number of neurons in each layer.

Step 3: Complete the training.

The Bayesian regularization algorithm is used as the learning algorithm for training.

Step 4: Verify the model.

The model is validated using different illumination waveforms and their corresponding internal residual electric fields. The verification signal requires to meet the sampling rate and spectral relationship described in Step 1.

3.3. Evaluation of Prediction Accuracy

In HEMP test analysis and effect evaluation, the most commonly used signal parameter is the amplitude of waveform. For the internal residual electric field, another parameter is the energy of the signal. Therefore, according to the research requirement of HEMP, this paper proposes the following two prediction accuracy evaluation parameters.

(1) The energy deviation is represented by err_{energy} as shown in Eq. (3).

$$err_{\text{energy}} = \sum_t [y^2(t) - y'^2(t)] / \sum_t y^2(t) \tag{3}$$

where $y(t)$ is the real output of the system, and $y'(t)$ is the training output of the neural network.

(2) The peak deviation is represented by $err_{\max}$ as shown in Eq. (4), where $||\ ||_\infty$ represents an infinite norm.

$$err_{\max} = \left| \|y(t)\|_\infty - \|y'(t)\|_\infty \right| / \|y(t)\|_\infty = \left| \max_t(|y(t)|) - \max_t(|y'(t)|) \right| / \max_t(|y(t)|) \tag{4}$$

4. INTERNAL RESIDUAL ELECTRIC FIELD MODELING BASED ON SIMULATION DATA

In this section, the EM simulation software CST is used to calculate the residual electric field inside the shield under specific illumination of HEMP. The training data for modeling and the validation data for model validation can then be obtained.

4.1. EM Simulation Modeling

In the simulation, the model is a metal shield with a square slot. To simulate a complex situation, a metal box is located near the aperture. The model is shown in Fig. 5. The shield is a perfect electric conductor (PEC) cube having a size of 1 m × 1 m × 1 m and a thickness of 0.001 m. The coordinate origin O is the geometric center of the shield. In the middle of a face parallel to the xOz plane, there is a square slot of 0.6 m × 0.6 m, and the slot is 0.005 m in width. Inside the shield, there is a PEC cube placed near the aperture, having a size of 0.3 m × 0.3 m × 0.3 m. The geometric center of the inner cube is $(0.2, -0.2, -0.2)$.

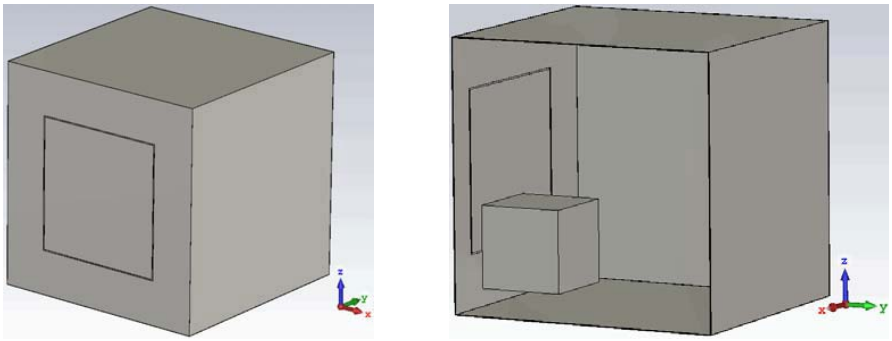

(a) (b)

Figure 5. Structure modeling of the shield. (a) Model of the shield. (b) Cutting position $x = 0.4$.

The simulation frequency range is 0–300 MHz. The internal residual electric field measurement point takes the inner geometric center of the shield.

The direction of incident EM wave is along the $+y$ direction. The direction of electric field is along the $-z$ direction. They are shown in Fig. 6.

The incident EM wave is the HEMP defined in IEC 61000-2-9, with $t_r = 2.5$ ns, $t_w = 23$ ns, as shown in Fig. 7(a). The HEMP waveform and internal residual electric field waveform, as shown in Fig. 7(b), obtained by EM simulation constitute the training data of the neural network.

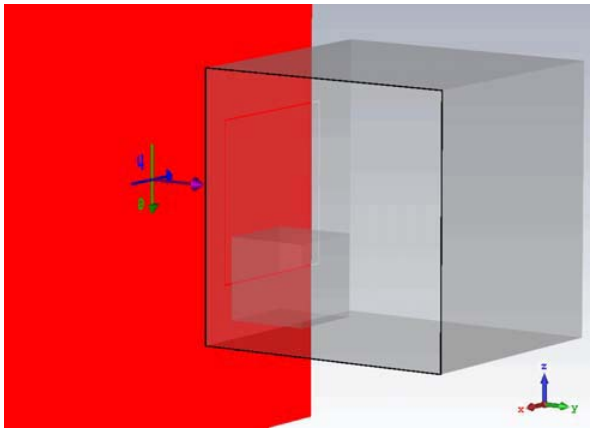

Figure 6. EM wave illumination direction and electric field direction.

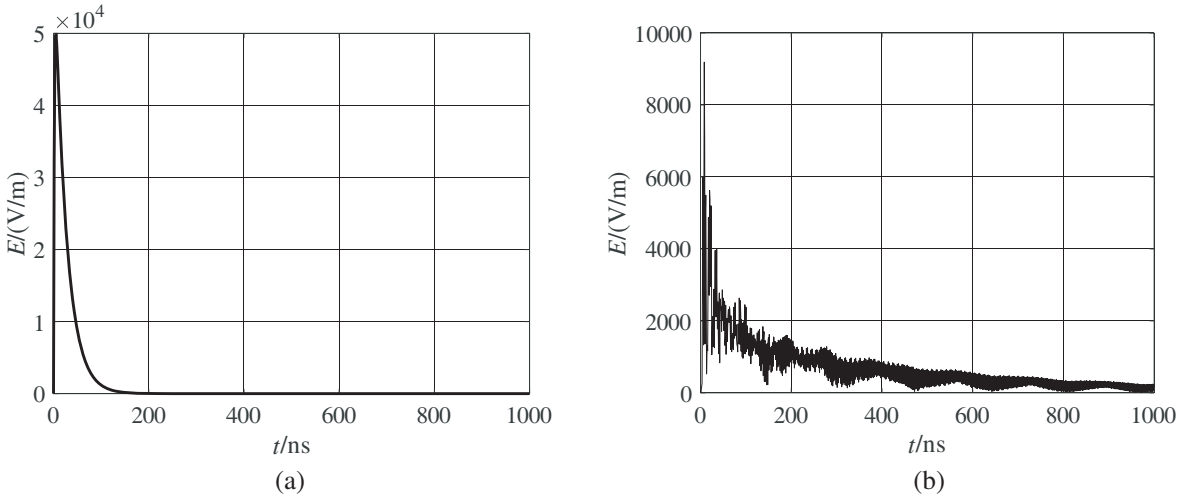

Figure 7. Simulation data obtained by HEMP illumination in accordance with IEC 61000-2-9. (a) Incident EM wave. (b) Internal residual electric field.

In the NARX neural network of this paper, the time delay of input and output signals is chosen as 10. The network has one hidden layer with 20 neurons. The determination of the values of these two parameters will be discussed later. The learning algorithm is BR algorithm. The iterative training completes the establishment of the NARX neural network.

To verify the model, parameters of the incident EM wave respectively satisfy Bell HEMP waveform and 1976 article waveform. The predicted and EM simulation waveforms are shown in Fig. 8. It can be seen from the results that NARX neural network can model the HEMP residual electric field inside EM shield. The prediction results are in good agreement with the simulation ones.

4.2. Prediction Accuracy

err_{energy} and $err_{\max}$ of the predicted residual electric field under different HEMP waveforms are shown in Table 1. For the convenience of expression, err_{energy} and $err_{\max}$ are given by percentage.

Analyzing the data in Table 1, it can be obtained that:

a. The $err_{\max}$ are all less than 5%. In actual analysis of the shielding performance of EM shield, the ratio of peak value of the electric field inside and outside EM shield is generally considered and expressed in the form of dB. Therefore, the impact of $err_{\max}$ on shielding performance analysis is less than 0.42 dB and can be ignored.

Table 1. Prediction accuracy of internal residual electric field under different HEMP waveforms.

Error	Bell	1976 article
err_{energy}	3.5%	22.8%
$err_{\max}$	3.7%	3.1%

b. The err_{energy} is less than 5% for Bell. It can meet the requirement of various HEMP analysis. The prediction error of the 1976 article is relatively large and a little more than 20%.

In summary, the two deviation indicators of Bell are sufficiently small to meet the general requirement of prediction accuracy. Although the err_{energy} of 1976 article is 22.8%, the $err_{\max}$ is sufficiently small for actual use. Thus, it can be seen from Fig. 8 and Table 1 that the generalization ability of the NARX neural network is strong in solving this problem. It is suitable for solving this kind of problems.

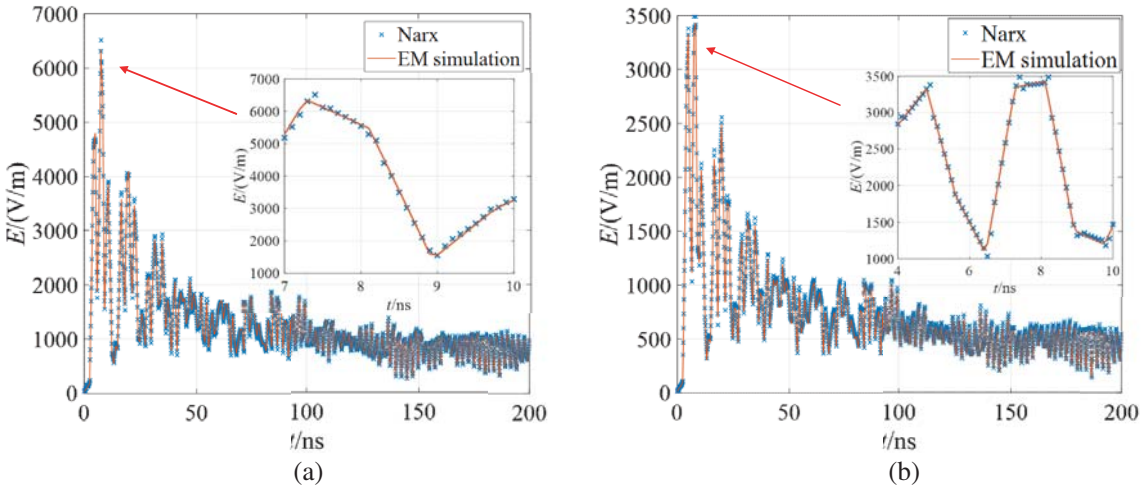

Figure 8. Comparison of predicted waveforms and simulated waveforms of residual electric field inside EM shield under the illumination of different HEMP waveforms. (a) Bell HEMP. (b) 1976 literature.

4.3. Determination of the Time Delay and Number of Neurons

In order to choose the proper time delay and number of neurons for the NARX neural network in this paper, the above simulations with different neural networks are carried out.

For the neural network in each simulation, time delay is chosen from 1 to 30, and number of neurons is chosen from 5 to 50. The verification with Bell HEMP waveform and 1976 article waveform is carried out to find the best value of the parameters, respectively. The simulations with different waveforms, time delays or numbers of neurons are regarded as different test statuses. The simulations are iterated for 100 times in one test status. The maximum $err_{\max}$ and err_{energy} of each test status are calculated to distinguish the proper value of time delay and number of neurons, as shown in Fig. 9.

After the analysis of Fig. 9 and the simulation data, 10 and 20 are chosen as the time delay and number of neurons respectively to get lower $err_{\max}$ and err_{energy}.

The typical number of iterations of the training is shown in Fig. 10. On average, it only requires less than 10 epochs for the network to be trained. The relative training performance is shown in Fig. 11. From the regression analysis of real and predicted values in Fig. 11, it can be seen that the regression line is close to $y = x$. There is almost no deviation from the straight line. The training performance is good for actual use.

The hardware configurations of the programs are: CPU: Intel i7-3770 3.4 GHz, RAM: 4 GB. The running time of the program is about 15 seconds.

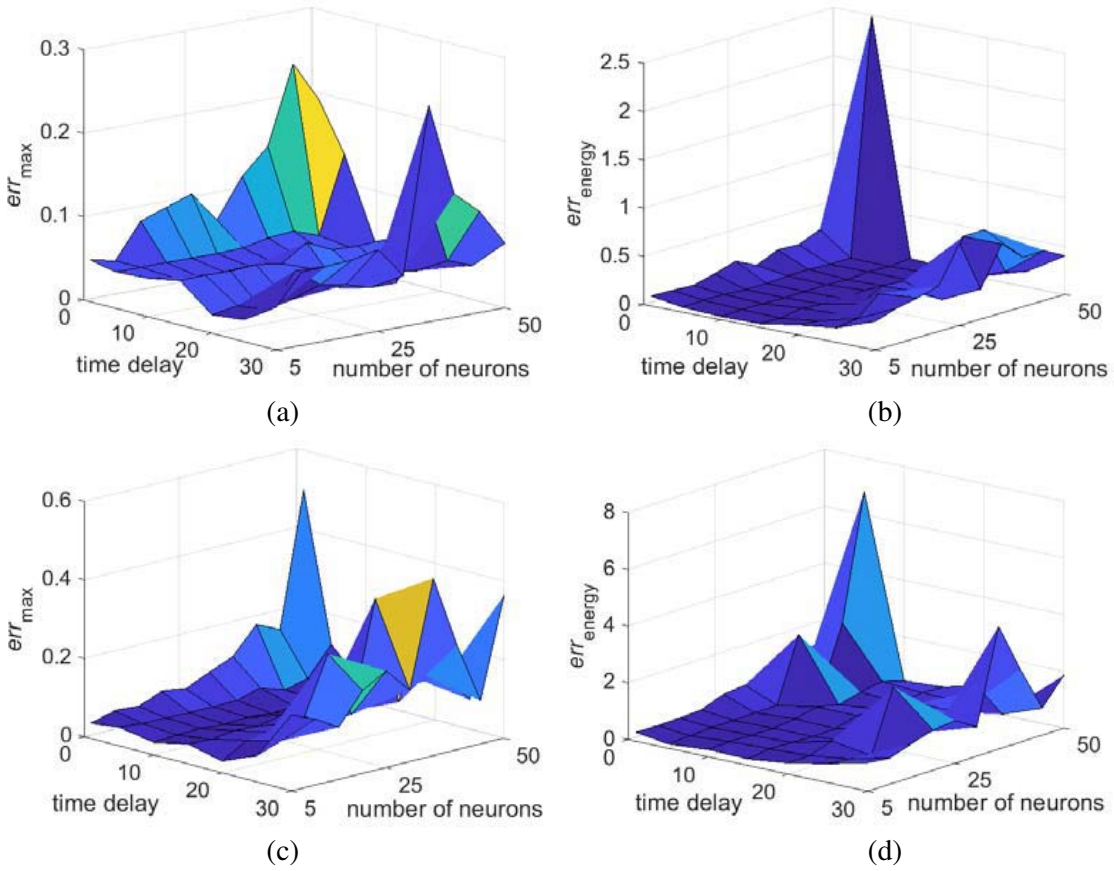

Figure 9. (a) $err_{\max}$ of Bell vs. time delay and number of neurons. (b) err_{energy} of Bell vs. time delay and number of neurons. (c) $err_{\max}$ of 1976 article vs. time delay and number of neurons. (d) err_{energy} of 1976 article vs. time delay and number of neurons.

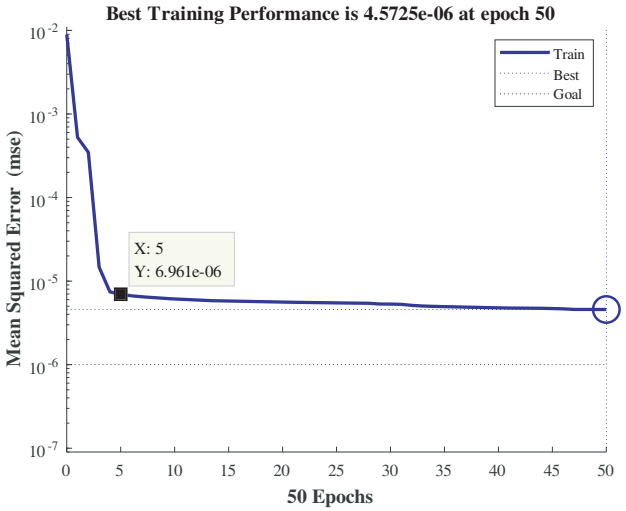

Figure 10. Typical number of iterations of the training of the NARX neural network.

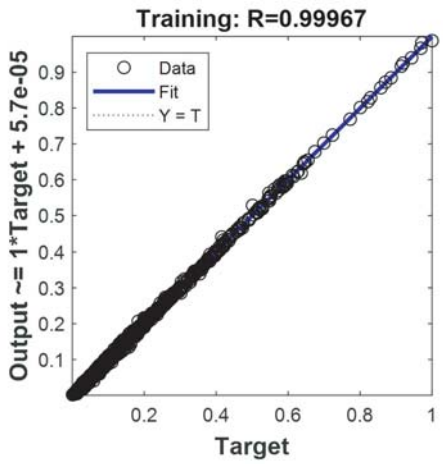

Figure 11. Training performance of the NARX neural network.

Based on these CST simulation data, it can be seen that the prediction error of the method base on NARX neural network is sufficiently small for actual use. As the value of the time delay and number of neurons are not very big, running speed of the programs is faster than the CST simulation mentioned above.

5. VERIFICATION BASED ON EXPERIMENT DATA

In this section, HEMP field test is carried out to verify the method proposed. All the waveforms of the incident EM environment are written as HEMP for simplicity in the following paragraphs.

A simple metal shield with a square slot is placed in the working volume of the HEMP simulator, illuminated by the HEMP environment, as shown in Fig. 12(a) and Fig. 12(b). The size of the shield is 1 m × 1 m × 1 m, and the thickness is 0.001 m. The size of the square slot is 0.6 m × 0.6 m, and it is 0.005 m in width. A metal box and a metal plate are randomly placed inside the shield, as shown in Fig. 12(c).

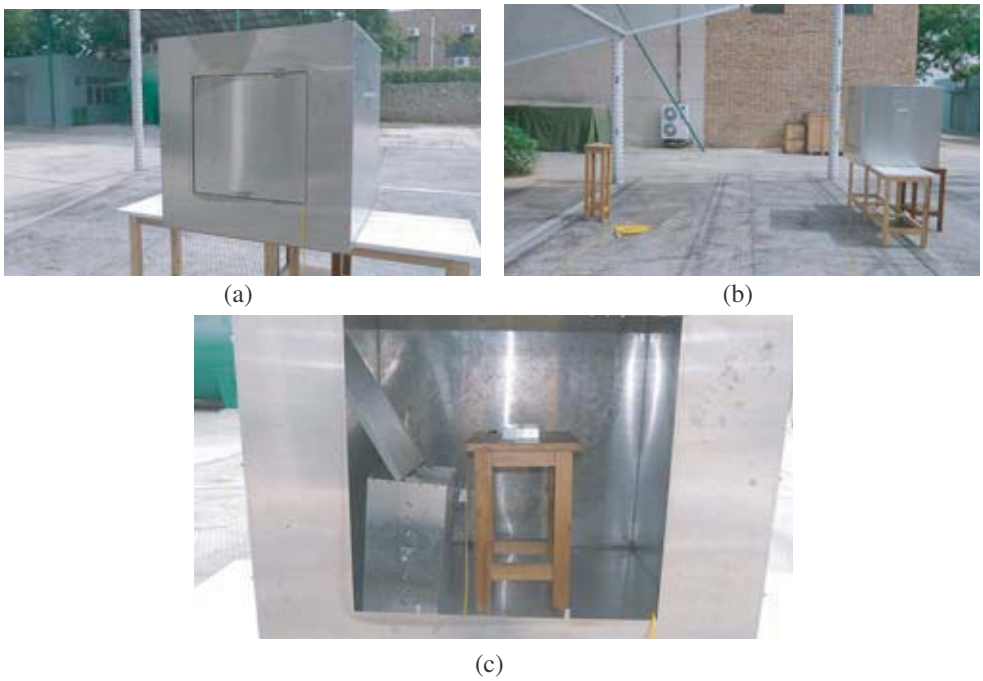

Figure 12. Experiment photographs of the EMP field test. (a) The metal shield with a square slot. (b) The shield placed in the working volume of the HEMP simulator. (c) The field sensor and other metal objects inside the shield.

A field sensor is placed in the geometric center of the shield to monitor only the z component of the EM environment inside the shield. Another field sensor placed outside the shield is used to monitor the HEMP environment and calculate the incident HEMP environment at the location of the shield.

The HEMP field tests of three different HEMP waveforms are carried out. The parameters of the incident HEMP waveforms are shown in Table 2. The HEMP waveforms are shown in Fig. 13. The basic requirements of spectrum coverage can be met between different incident HEMP waveforms, as shown in Fig. 14. The high-frequency component above 100 MHz is very small to the field sensor, compared to the low-frequency component. Hence, the high frequency part of the waveform is almost all noise. The waveforms inside the shield are shown in Fig. 15. The waveforms in frequency domain are shown in Fig. 16. In the three tests, the EM waveforms inside the shield are quite different from each other both in time domain and frequency domain.

In the NARX neural network of this section, the time delays of input and output signals are also

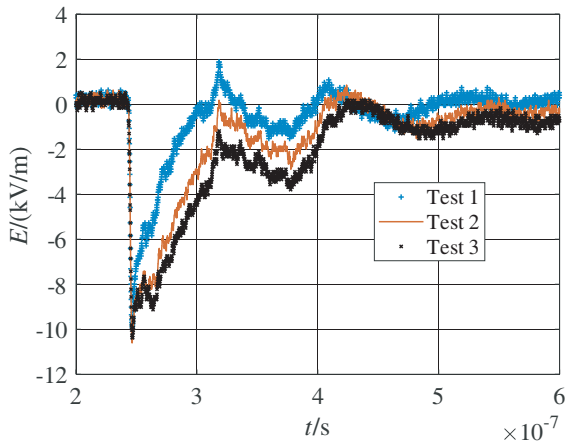

Figure 13. The waveforms of the incident HEMP environment.

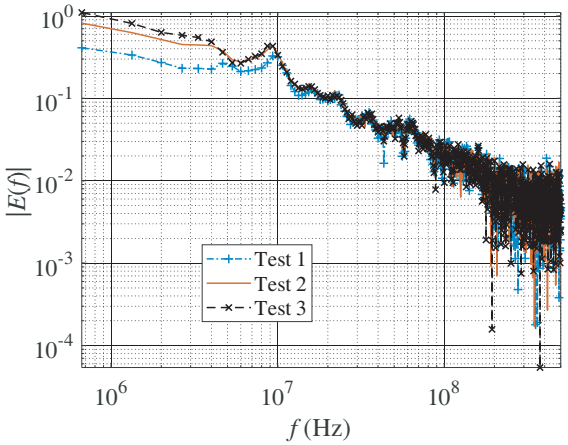

Figure 14. The waveforms of the incident EMP environment in frequency domain.

Table 2. Parameters of the different EMP waveforms.

Test ID	Amplitude of the incident HEMP waveform (kV/m)	t_r (ns)	t_w (ns)
Test 1	10.1	1.8	21.6
Test 2	10.8	1.9	36.0
Test 3	10.6	2.1	46.3

chosen as 10. The network has one hidden layer with 20 neurons. The learning algorithm is BR algorithm. The iterative training completes the establishment of the NARX neural network.

The data of the three tests are composed of the EMP environment E_{os} at the location of the shield and the EM environment E_{is} at the center inside the shield. E_{os} and E_{is} of Test 1 are used as the training data of the NARX neural network. E_{os} is the input data. E_{is} is the output data. The data of Test 2 and Test 3 are input into the trained NARX neural network respectively for verification. The output of the network is compared with E_{is} of Test 2 and Test 3.

The comparison of Test 2 is shown in Fig. 17. Fig. 17(a) is partially enlarged for a better view, as shown in Fig. 17(b). The prediction accuracy is: $err_{\text{energy}} = 0.5\%$ and $err_{\max} = 3.0\%$. The comparison of Test 3 is shown in Fig. 18. Fig. 18(a) is partially enlarged for a better view, as shown in Fig. 18(b). The prediction accuracy is: $err_{\text{energy}} = 1.4\%$ and $err_{\max} = 0.9\%$. As shown in Figs. 17–18, the prediction waveforms are in good agreement with the test data. The two deviation indicators are sufficiently small to meet the general requirement of prediction accuracy.

This research has a very important role in HEMP coupling analysis of complex EM shields and even the situation of "black box". Compared to numerical simulation, the proposed method can predict the results through the measured data, without the information about the structure of EM shield. Due to the use of test data, it can be more accurate than EM numerical methods. The comparison between the measurement data of Test 2 and CST simulation data is shown in Fig. 19. The parameters of the illuminated waveform in CST simulation are the same as in Test 2. The model is built with reference to the real shield. However, some details are omitted, as can be seen from Fig. 12 and Fig. 20. The difference of the two waveforms in Fig. 19 is mainly caused by the missing of these details.

Compared to HEMP field tests, the prediction error of the method proposed in this paper is acceptable. It is common that the fluctuation of the illuminated HEMP environment sometimes can reach 10%–20%. The uncertainty of the measurements of coupling currents and electric fields is commonly about 5% or higher. So the prediction accuracy of the NARX neural network can meet the actual requirements. Compared to real tests, there is another advantage of the method. Changing parameters of the illuminated waveform to a specific value is difficult for HEMP simulator. It is

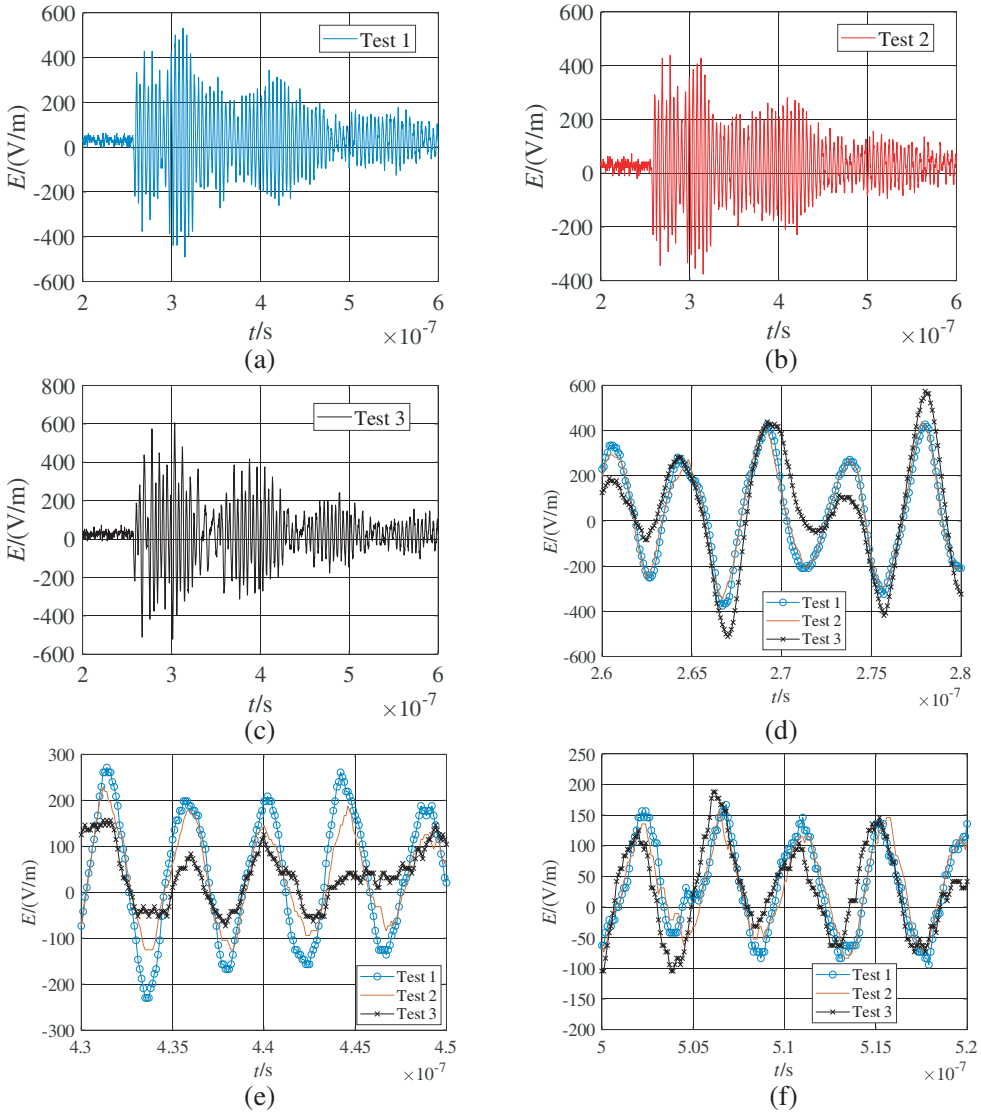

Figure 15. The waveforms of the monitored EM environment inside the shield. (a) Test 1. (b) Test 2. (c) Test 3. (d) The comparison of the waveforms with t from 2.6–2.8 $\times 10^{-7}$ s. (e) The comparison with t from 4.3–4.5 $\times 10^{-7}$ s. (d) The comparison with t from 5.0–5.2 $\times 10^{-7}$ s.

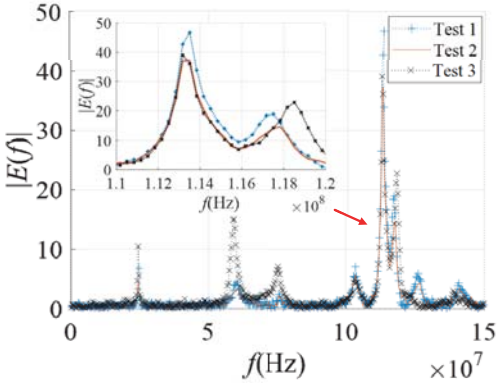

Figure 16. The waveforms of the monitored EM environment inside the shield in frequency domain.

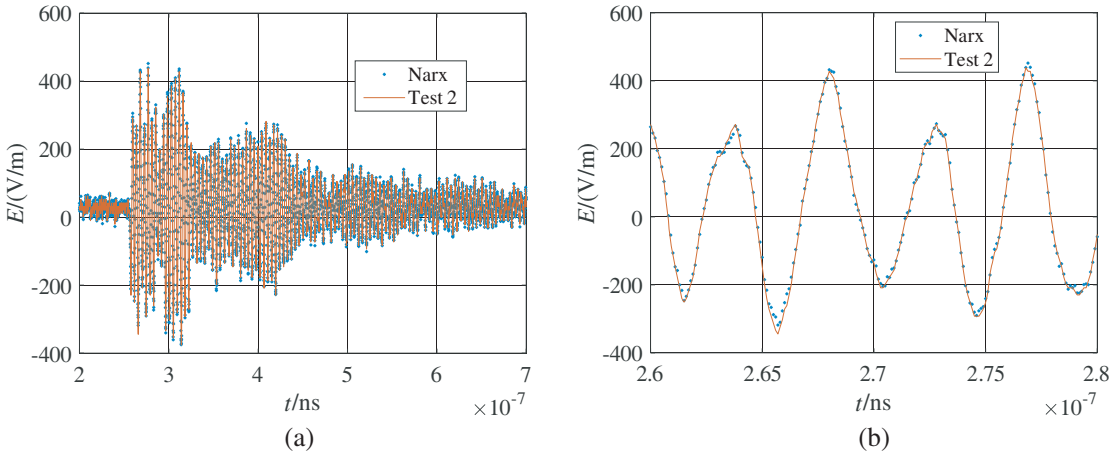

Figure 17. The predicted waveform of NARX neural network and the real test measurement data E_{is} of Test 2. (a) The normal view. (b) The partially expanded view.

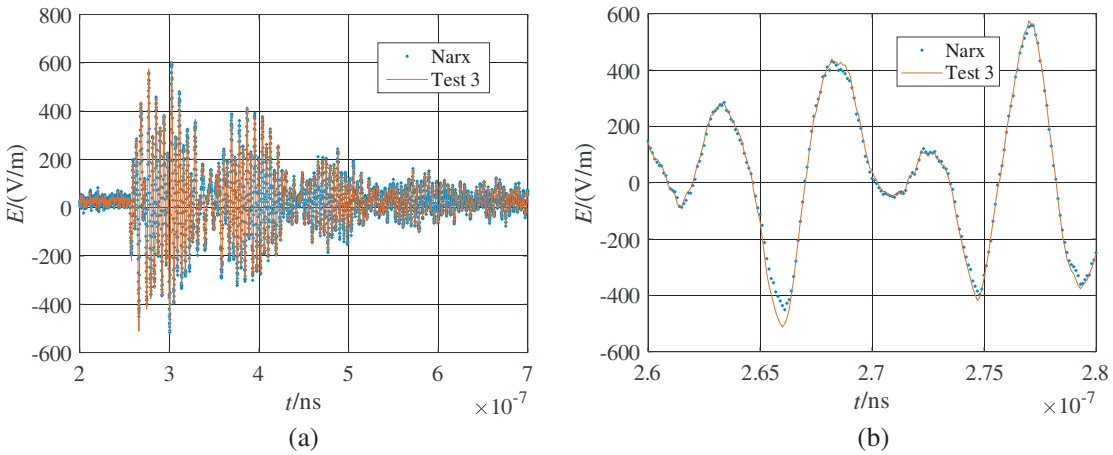

Figure 18. The predicted waveform of NARX neural network and the real test measurement data E_{is} of Test 3. (a) The normal view. (b) The partially expanded view.

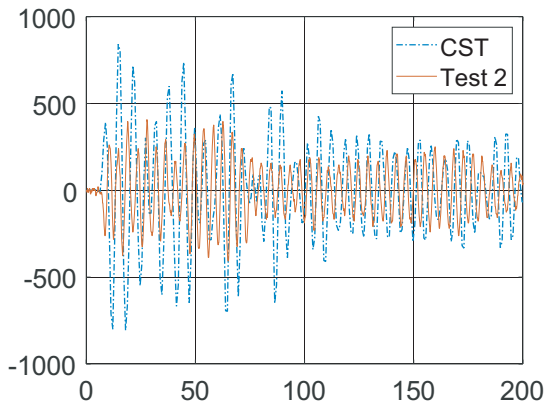

Figure 19. The comparison between the measurement data of Test 2 and the simulation data of CST.

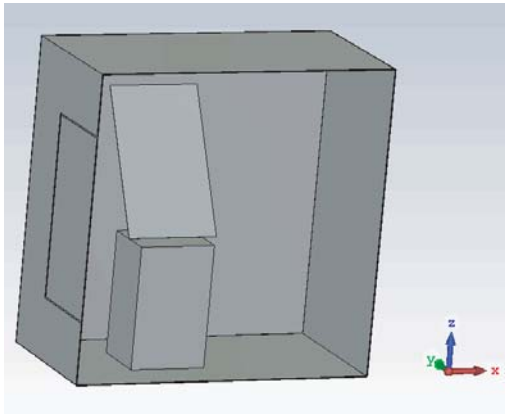

Figure 20. CST model of the shield in Test 2.

expensive and time consuming. However, the model based on NARX neural network can easily solve these problems.

6. CONCLUSION

This paper mainly studies the prediction of residual electric field inside EM shield under the illumination of different HEMP waveforms. Based on NARX neural network, the prediction model is established according to the data of a HEMP waveform and its corresponding residual electric field. The model is then used to predict the residual electric field inside EM shield under the illumination of other HEMP waveforms. The verification of the model is completed through EM simulation and HEMP field test.

However, the series-parallel architecture of NARX neural network can only predict the output of the next one time step. Compared to series-parallel architecture, the NARX neural network based on parallel architecture can be directly used in test analysis, evaluation of HEMP residual electric field test, and EM shield design. However, it is commonly not stable and hard to train. So in practice, establishing the series-parallel architecture is commonly the first step. The second step is closing the loop of series-parallel architecture to create the parallel architecture. The network would be retrained depending on the actual performance. So based on the network proposed in this paper, the future work will be concentrated on studying the stability of parallel architecture for these problems.

REFERENCES

1. Donald, R. V., "Electromagnetic pulse effects on a typical electric utility system," *IEEE Trans. on Power Apparatus & Systems*, Vol. 103, 2215–2221, 1984.
2. Liu, H., Y. Xi, and J. Yang, "Electromagnetic pulse effect analysis for doppler radar," *Journal of Microwaves*, Vol. S3, 309–311, 2012.
3. Kichouliya, R. and M. J. Thomas, "Interaction of high power electromagnetic pulses with power cables and electronic systems," *IEEE International Symposium on EMC*, 159–163, Jul. 2016.
4. Zhou, B., B. Chen, and L. Shi, *EMP and EMP Protection*, 288–289, National Defense Industry Press, 2003.
5. Liu, S., J. Liu, and X. Dong, *Electromagnetic Shielding Effectiveness and Radar Absorbing Material*, 83–86, Chemical Industry Press, 2007.
6. Kuo, C. and C. Kuo, "Finite-difference time-domain analysis of the shielding effectiveness of metallic enclosures with apertures using a novel sub gridding algorithm," *IEEE Trans. on Electromagnetic Compatibility*, Vol. 58, No. 5, 1595–1601, 2016.
7. D'Amore, M. and M. S. Sarto, "Theoretical and experimental characterization of the EMP-interaction with composite-metallic enclosures," *IEEE Trans. on Electromagnetic Compatibility*, Vol. 42, No. 2, 152–163, 2000.
8. Araneo, R. and G. Lovat, "An efficient MoM formulation for the evaluation of the shielding effectiveness of rectangular enclosures with thin and thick apertures," *IEEE Trans. on Electromagnetic Compatibility*, Vol. 50, No. 2, 294–304, May 2008.
9. Carpes, Jr., W. P., G. S. Ferreira, A. Raizer, L. Pichon, and A. Razek, "TLM and FEM methods applied in the analysis of electromagnetic coupling," *IEEE Trans. Magn.*, Vol. 36, No. 4, 982–985, Jul. 2000.
10. Rabat, A., P. Bonnet, K. E. K. Drissi, and S. Girard, "Analytical formulation for shielding effectiveness of a lossy enclosure containing apertures," *IEEE Trans. on Electromagnetic Compatibility*, Vol. 60, No. 5, 1384–1392, 2018.
11. Ianoz, M., "A review of HEMP activities in Europe (1970–1995)," *IEEE Trans. on Electromagnetic Compatibility*, Vol. 55, No. 3, 412–421, 2013.
12. Luo, M. and K.-M. Huang, "Prediction of the electromagnetic field in metallic enclosures using artificial neural networks," *Progress In Electromagnetics Research*, Vol. 116, 171–184, 2011.
13. Tahar Belkacem, F., M. Bensetti, M. Laour, A. Boutar, M. Djennah, D. Moussaoui, and B. Mazari, "The analytical, numerical and neural network evaluation versus experimental of electromagnetic

shielding effectiveness of a rectangular enclosure with apertures," *IEEE International Conference on Cybernetic Intelligent Systems (CIS 2010)*, Sept. 2010.

14. "Electromagnetic Compatibility (EMC)-Part 2: Environment — Section 9: Description of HEMP environment-radiated disturbance," IEC 61000-2-9 Ed. 1.0, 1996–2002.
15. Yu, S., "NEMP and NEMP protection," M.S. Thesis, Dept. Mechantron. Eng., Xidian University, Xi'an, China, 2008.
16. Tesche, F. M., "A multi conductor model for determining the response of power transmission and distribution to HEMP," *IEEE Trans. on Power Delivery*, Vol. 4, No. 3, 1955–1964, 1989.
17. Ricketts, L., W. J. E. Bridges, and J. Miletta, *EMP Radiation and Protective Techniques*, Wiley, New York, 1976.
18. Chen, S., X. X. Wang, and C. J. Harris, "NARX-based nonlinear system identification using orthogonal least squares basis hunting," *IEEE Transactions on Control Systems Technology*, Vol. 16, No. 1, 78–84, 2008.
19. Haykin, S., *Neural Networks and Learning Machines*, 3rd Edition, China Machine Press, 2011.
20. Hirschen, K. and M. Schafer, "Bayesian regularization neural networks for optimizing fluid flow processes," *Computer Methods in Applied Mechanics and Engineering*, Vol. 195, 481–500, 2006.
21. MacKay, D. J. C., "A practical Bayesian framework for back propagation networks," *Neural Comput.*, Vol. 4, No. 3, 448–472, May 1992.
22. Khafaf, N. A. and A. El-Hag, " Bayesian regularization of neural network to predict leakage current in a salt fog environment," *IEEE Trans. on Dielectrics and Electrical Insulation*, Vol. 25, No. 2, 686–693, 2018.